Journal of Bio- and Tribo-Corrosion (2023) 9:59
https://doi.org/10.1007/s40735-023-00775-4

Experimental and Theoretical Studies on Corrosion Inhibition of Mild Steel in Molar Hydrochloric Acid Solution by a Newly Benzimidazole Derivative

Nadia Jaàfar[1,2] · Habib El Alaoui El Abdallaoui[1] · Hassan El Attari[2] · Abdelmalek Matine[1] · Moutie Mohamed Rguiti[4] · Houssine Ait Sir[3] · Said Jebbari[3] · Mustapha Hilali[4]

Received: 28 January 2023 / Revised: 14 May 2023 / Accepted: 13 June 2023 / Published online: 27 June 2023

Abstract
In the present work, a new benzimidazole derivative, namely 1, 5-bis-2-[benzimidazol-2-yl] mercapto diethylene glycol (OSBZ) was synthesized and examined as a corrosion inhibitor for mild steel (MS) of type C38 in a very aggressive medium (1 M HCI) using weight loss and electrochemical (PDP and EIS) techniques, the surface of the metal was characterized by EDX, and SEM. The reagents used in the synthesis of OSBZ are available, their synthesis yield is important, and is characterized by ^{1}H, ^{13}C NMR and FTIR. The OSBZ is applicable in therapeutic chemistry. It was found that the inhibitory efficiency increases with the concentration of OSBZ to reach a maximum value of 94.78% for the concentration 3×10^{-4} M. The temperature effect on the inhibition performance was studied in the interval (298–318 K) and OSBZ adsorption on the surface of MS in the corrosive environment followed the Langmuir isotherm. The results were supported by density functional calculations (DFT) and molecular dynamics simulation (MD).

Keywords Corrosion inhibition · C38 steel · Benzimidazole's derivatives · Electrochemical test · DFT · MD

1 Introduction

Mild steel (MS) is a popular iron alloy, the least expensive and most mechanically resistant, which explains its numerous industrial applications, from building to installations such as nuclear power plants, chemical plants, oil installations. However, MS is very susceptible to corrosion, a problem of great concern to manufacturers [1]. In industrial processes, the use of steel hydrochloric acid is very frequent [2–6].

Corrosion is a natural process that causes the degradation of metals and alloys by chemical or electrical interaction with their environment [7].

Inhibition by organic compounds remains an adequate remedy. Several organic compounds have double bonds and contain heteroatoms such as nitrogen, sulfur, oxygen or phosphorus, functional groups such as –OH, –COOH, $–NH_2$, (acids, amino acids, amines, phenols….)these active polar groups play an important role in adsorption of inhibitory molecules in neutral form or in the form of ions on the metal surface [8]. The determination of the types of interactions between the inhibitor molecule and the metal surface is influenced by several parameters such as the physical and chemical properties of the molecule, the metal surface, and the electrolyte medium.

Organic corrosion inhibitors to protect iron and its alloys in acidic environments are numerous, particularly benzimidazoles. A group of studies showed that different types of benzimidazoles and its derivatives are good corrosion inhibitors in the extremely corrosive medium [9], based on the structure spatial molecular structure, surface charge density,

✉ Nadia Jaàfar
nadiajafaro@yahoo.fr

1 Molecular Modeling and Spectroscopy Research Team, Faculty of Sciences, Chouaib Doukkali University, PB 20, 24000 El Jadida, Morocco

2 Laboratory of Coordination and Analytical Chemistry, Faculty of Sciences, Chouaib Doukkali University, PB 20, 24000 El Jadida, Morocco

3 Bioorganic Chemistry Laboratory, Faculty of Sciences, Chouaib Doukkali University, PB 20, 24000 El Jadida, Morocco

4 Applied Chemistry-Physics Team, Faculty of Sciences, University of Ibn Zohr, Agadir, Morocco

electronic parameters and their affinity for the metal [6, 10]. We mention for example a saline environment (NACE brine ID196 and 3% NaCl) [10, 11], and the acidic medium (10–20–30% acetic medium; 0.5 M H_2SO_4; 1 M HNO_3) [12–14] (1–0.5–0.1 M HCl) [15–17]. The metals used are as diverse as mild and carbon steel, steels, pure metals such as Zn, Al, Fe, Cu and alloys [6, 14, 18–21].

The inhibitory efficiency reaches important values for these different materials in different media. In particular for MS and in 1 M HCl medium, the inhibitory efficiency of some benzimidazole derivatives reaches 97% and 98% [22–25].

Considerable attention has been paid to benzimidazoles because they represent an important multiple biological activities as antimicrobial, anti-inflammatory, analgesic, antidiabetic, anticonvulsant, antioxidant, antiulcer, antihypertensive, antiparasitic, antiviral and anticancer activities [26].

The search for new benzimidazole derivatives is still experiencing a very significant growth based on applications a large number of fields especially biological and industrial. The present study aims to correlate the molecular structure of the newly benzimidazole derivative OSBZ and its effectiveness in inhibiting the iron corrosion in an acid environment. The inhibitory action was evaluated using electrochemical techniques (polarization curves, impedance spectroscopy) by the gravimetric method, and scanning electron microscopy (SEM). These techniques enabled us to determine the inhibitory effect of this compound, its mode of action and certain parameters specific to corrosion. The interpretation of the inhibiting power is explained using quantum calculation.

2 Experimental Procedure

2.1 Materials, Specimens, and Electrolyte

The composition of C38 is summarized in Table 1.

The MS specimens were abraded using (400–1200 grade) emery paper, washed with distilled water, and degreased with acetone, and finally air-dried. By dilution of the commercial hydrochloric acid (37%) with distilled water, we prepared the corrosive medium (1 M HCl).

2.2 Synthesis of Inhibitor

Chemicals and solvents for this study were obtained from Aldrich and of analytical grade. Into a 50 ml Erlenmeyer flask, (0.01 mol) of benzimidazole-2-thiones, (0.005 mol) bis(chloroethyl) ether or 1, 2-bis (2-chloroethoxy) ethane (0.02 mol) of potassium bicarbonate (K_2CO_3), and 20 ml of dimethyl formamide (DMF) were introduced. The mixture is left under magnetic stirring, at room temperature for 72 h. The progress of the reaction is followed by thin layer chromatography. After stopping the reaction, water was added to the reaction mixture, which resulted in the appearance of a white precipitate. The precipitate, thus obtained, was filtered, wrung out and dried in the oven. The crude product is then recrystallized in ethanol and filtered to give compound OSBZ ($C_{18}H_{22}N_4OS_2$; MW = 370 g/mol), this reaction is summarized in Fig. 1.

For categorized each compounds used NMR, IR and mass spectra. The following instruments were used: melting points (Köfler Apparatus, uncorrected); IR spectra (FTIR Shimadzu, 4000–400 cm^{-1}); NMR spectra (Bruker ARX 200, 200 MHz for ^1H and 50.3 MHz for ^{13}C, δ ppm/TMS, J in Hz); mass spectra (Varian MAT 311A, EI); column chromatography (silica gel 60, 230–400 mesh).

The structure of compound OSBZ established on the basis of NMR spectral data of proton and carbon 13. The spectroscopic characteristics of the product are as follows: The NMR spectrum of compound OSBZ shows two triplets at 3.44 and 3.74 ppm corresponding to the methylene

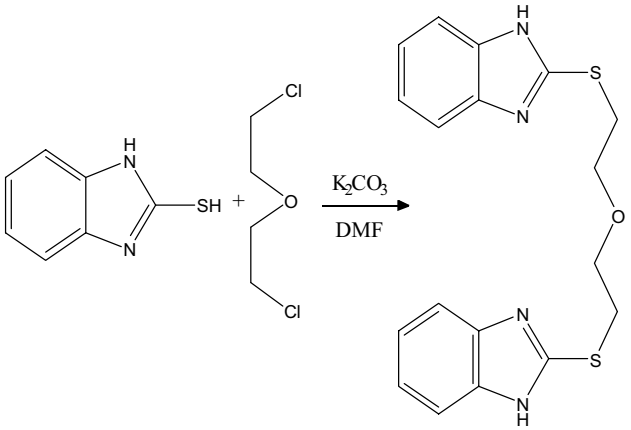

Fig. 1 Synthesis of 1.5-bis-2-[benzimidazol-2-yl] mercapto diethylene glycol

Table 1 Nominal composition of used C38

Elements	Fe	Si	C	Mn	S	P
Content (%)	Balance	0.16	0.38	0.41	0.02	0.01

groups, a mass corresponding to the 3 aromatic protons centered at 6.98 ppm, another corresponding to an aromatic proton centered at 7.27 ppm and a singlet at 12.58 ppm corresponding to the proton bound to nitrogen.

Yield = 69% as a white solid, m.p. 225 °C.

2.2.1 ^{1}H-NMR (DMSO-d_6/TMS)

3.44 (t, SCH_2CH_2, $^{3}J_{HH}$ = 6.0 Hz), 3.74 (t, OCH_2CH_2–, $^{3}J_{HH}$ = 6.0 Hz), 7.27 (m, 1H), 6.98 (m, 1H), 12.58 (s, NH).

2.2.2 ^{13}C-NMR (DMSO-d_6/TMS)

31.7. (t, SCH_2CH_2), 70.1 (t, OCH_2CH_2), 109.6 (CH), 113.6 (CH), 122.4 (CH), 122.5 (CH), 132.4, 134.6, 149.7 (C_2).

2.2.3 IR (KBr)

3380, 2870, 1584, 1450, 1297, 1198 cm^{-1}; MS [*m*/*z*, (%)]: 370 $[M]^+$ [27].

2.3 Gravimetric Measurements

It consists in measuring the mass loss Δm of the surface samples S during the time t immersion of the sample in a corrosive solution. The corrosion rate is given by the relation: $W = \frac{\Delta m}{S.t}$.

The inhibitory efficacy of an organic compound is determined by the following relationship [28]:

$$\mathrm{IE}(\%) = \frac{W - W_{\mathrm{inh}}}{W} \times 100,$$

where W and W_{inh} are the corrosion rates respectively in the absence and in the presence of the inhibitor.

The MS samples used, rectangular in shape and measuring 1 cm × 2 cm are prepared, weighed, and immersed in an inclined position for 6 h in the corrosive solution, in the absence of agitation, and maintained at a constant temperature (25 °C). At the end of the experiment, the corrosion products are discarded and the samples are weighed again.

The main disadvantage of this method lies in the difficulty of completely eliminating the corrosion products without removing unattacked metal.

2.4 Electrochemical Methods

Electrochemical methods allow the characterization of the metal/electrolyte interface. We can classify these methods according to two main categories: stationary and transient methods. The application of electrochemical techniques offers several advantages. In particular, it is noted that electrochemical methods provide information concerning the activities of chemical species rather than their concentrations. Indeed, the electrochemical methods used to characterize the metal/electrolyte interface [29] are based on the drawing of polarization curves on a logarithmic scale, which allows us to directly access the value of the corrosion current, and transient electrochemical methods among which electrochemical impedance measurements. The transient electrochemical technique is still a relevant method to study the mechanism that takes place at the metal/electrolyte interface, based on the analysis of the double layer formed at the MS/electrolyte interface [30]. The experimental device used for all the stationary and transient tests is a voltalab potentiostat controlled by a computer using Versastudio software. The cell is thermostatically controlled and double-walled containing three electrodes, a C38 steel working electrode with a surface area of 0.27 cm^2, a platinum counter electrode and a saturated calomel electrode (SCE) as reference electrode. Before each electrochemical test the surface of the working electrode it undergoes polishing with abrasive paper with a grain size of up to 1200, then it is rinsed with distilled water and dried with hot air. The working electrode is subjected to its free corrosion potential for 30 min under normal ventilation conditions at the chosen temperature. For the polarization measurement the cathodic and anodic curves were scanned from − 900 to − 100 mV/SCE with a scan rate 1 mV/s. For the impedance study we used a frequency range from 10,000 Hz to 0.01 Hz with a wave amplitude of 10 mV.

2.5 Surface Analysis: SEM, EDX

The surface analysis of modified samples was characterized by field-emission SEM (JEOL JSM 6480LV) at an energy of 20 kV.

The C38 samples were immersed in the 1 M HCl containing and lacking an optimum concentration of OSBZ for 6 h at 298 K.

2.6 Molecular Modeling

2.6.1 Quantum Chemistry Calculations

The GAUSSIAN 09W program [31] and Gauss View 5.0.8 software were used for all quantum chemistry computations and result display. The calculated vibrational frequencies are calculated using the DFT (density functional theory) method at the B3LYP (Becke-3-parameter-Lee–Yang–Parr) level with the 6-311G (d,p) basis in the aqueous state to produce the optimal geometrical structure of the studied molecules [32].

The energy of the most occupied molecular orbital (E_{HOMO}) and the energy of the lowest unoccupied molecular orbital (E_{LUMO}) were used to calculate the quantum chemical parameters, including the energy gap (ΔE_{gap}), absolute

electronegativity (χ), absolute hardness (η), softness (σ), overall electrophilicity index (ω), and fraction of transferred electrons (ΔN) [33], using the following Eqs. 1–6.

$$\Delta E_{GAP} = E_{LUMO} - E_{HOMO}, \tag{1}$$

$$\eta = (E_{LUMO} - E_{HOMO})/2, \tag{2}$$

$$\sigma = 1/\eta, \tag{3}$$

$$\chi = -(E_{LUMO} + E_{HOMO})/2, \tag{4}$$

$$\omega = \chi^2/2\eta, \tag{5}$$

$$\Delta N = (\emptyset_{Fe} - \chi_{inh})/2(\eta_{Fe} + \eta_{inh}), \tag{6}$$

where $\emptyset_{Fe}$ is the work function of the iron, and χ_{inh} is the absolute electronegativity of the inhibitor molecule, η_{Fe} and η_{inh} are the overall hardnesses of iron and the inhibitor molecule, respectively. Using a theoretical value of the work function of iron equal to $\emptyset_{Fe} = 4.82$ eV [34]. and an overall hardness at $\eta_{Fe} = 0$ eV for the calculation of the fraction of transferred electrons [35].

2.6.2 Fukui Functions and Locale Reactivity

Condensed Fukui functions have been elucidated toward an understanding many information's about local reactivity. The finite difference approximation can be used to determine the nucleophilic f^+ and electrophilic f^- Fukui functions, which are responsible for the change in electron density. These induces were calculated using the following Eqs. 7–8.

$$f^+ = q(N+1) - q(N), \tag{7}$$

$$f^- = q(N) - q(N-1), \tag{8}$$

where $q(N)$, $q(N+1)$ and $q(N-1)$ are the electronic population of the atom in neutral, anionic and cationic systems, respectively [36].

2.6.3 Molecular Dynamics Simulations

The Materials Studio program 7.0 created by Accelrys, Inc., was applied to simulate the molecular dynamics (MD) simulations [37]. We used two modules in this study. First one, the molecular structure of the inhibitor is geometrically fully optimized using the Forcite module, then, the adsorption localization module was used to identify the possible adsorption configurations mechanism. In this study, for the MD simulations of the interaction between the molecule inhibitor and the iron surface of Fe, a simulation box of three-dimensional geometry with dimensions (17.20 22.93 22.93) was utilized (110) [38]. The equations of motion were integrated using the canonical set NVT and the periodic boundary conditions were employed in all three directions. The Fe layer, the water layer containing the studied inhibitor and a vacuum layer were included in the simulation box. We used the COMPASS force field with a time step of 0.1 fs and a simulation time of 15 ps while working at a temperature of 293 K adjusted by the Noze technique [39].

The following expression (Eq. 9) was used to evaluate the interaction energy ($E_{interaction}$) between the inhibitor molecule and the surface of Fe (110).

$$E_{interaction} = E_{total} - (E_{surface} + E_{inhibitor}) \tag{9}$$

such as: $E_{binding} = -E_{interaction}$

E_{total}: the total energy of the simulation system.

$E_{surface}$: the energy of the iron surface together with H_2O molecules.

$E_{inhibitor}$: the energy of the free inhibitor molecule.

3 Results and Discussion

3.1 Weight Loss Measurements

The W and IE (%) without and with OSBZ of various concentrations (5×10^{-5} to 3×10^{-4} M) in 1 M HCl solution at 298 K were calculated using of the weight loss experiments (WL), the results represented in Table 2 show that after adding the OSBZ molecule the w values are decreasing and IE are increasing. The OSBZ showed the best IE of 94.78% at 3×10^{-4} M. when the concentration of the inhibitor in the corrosive solution increases the coverage of the surface of the metal increases hence the increase in the inhibition efficiency [40].

Table 2 Corrosion rate and inhibition efficiency at various concentrations of OSBZ in 1 M HCl at 298 K

Concentration (M)	W (mg/cm^2/h)	I E(%)
Blank	0.46	–
5×10^{-5}	0.075	83.69
10^{-4}	0.048	90.65
2×10^{-4}	0.043	92.39
3×10^{-4}	0.024	94.78

3.2 Electrochemical Study

3.2.1 Potentiodynamic Polarization (PDP)

Figure 2 illustrates the polarization curves of MS in HCl (1 M) at 25 °C without and with addition of the compound at concentration between 5×10^{-5} and 3×10^{-4} M. The setting electrochemical deduced from these curves are reported in Table 3.

The inhibition efficiency of an organic compound is determined by the following relationship (Eq. 10) [41]:

$$\mathrm{IE}(\%) = \frac{I_{\mathrm{corr}} - I_{\mathrm{corrinh}}}{I_{\mathrm{corr}}} \times 100, \tag{10}$$

where I_{corr} and I_{corrinh} are the corrosion current density in the absence and in the presence of the inhibitor, respectively.

The first remark is that the nature of the anodic and cathodic Tafel curves was affected by the addition of OSBZ inhibitor, implying that the anodic dissolution of C38 is done slowly, and also at cathode, the release of hydrogen gas is reduced [42–44]. The cathodic evolution of hydrogen can be explained by the following mechanism [2]:

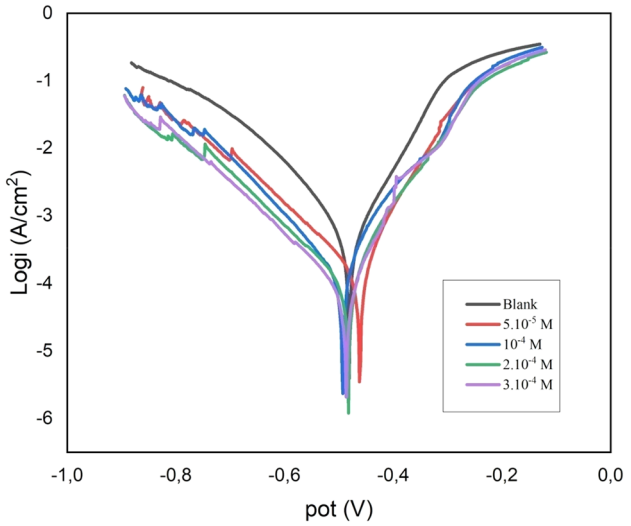

Fig. 2 Polarization curves of MS in 1 M HCl without and with addition of OSBZ at different concentrations at 298 K

$$\mathrm{FeH}_{(\mathrm{ads})} + \mathrm{H}^{+} + \mathrm{e}^{-} \rightarrow \mathrm{Fe} + \mathrm{H}_{2}.$$

The anodic dissolution of iron can be expressed as follows [2]:

$$\mathrm{FeCl}^{+}_{(\mathrm{ads})} \leftrightarrow \mathrm{Fe}^{2+} + \mathrm{Cl}^{-}.$$

In the anodic domain, we note that beyond − 250 mV the presence of the OSBZ no longer has any effect on the anodic dissolution, suggesting a desorption of this inhibitor. The variation of the corrosion potential with variation of concentration is very little, it is equal to the maximum $\Delta E_{\mathrm{corr}} = 34.87$ mV, meaning that The compound OSBZ can be classified as mixed inhibitor in 1 M HCl with a cathodic predominance [45, 46].

The examination of Fig. 2 and Table 3 shows that the cathodic curves present a range where the log I vary linearly with E, implying that Tafel's law hold in the cathodic domain. Thus, the discharge of the proton H^+ on the surface of the steel is done according to a mechanism pure activation, also the Tafel cathodic slope (β_c) shows a slight modification with the addition of the inhibitor tested in this corrosive medium indicating that the hydrogen reduction mechanism is not affected by OSBZ [25]. The inhibition efficiency reaches 84.86% with a low concentration OSBZ (3×10^{-4} M) indicating that OSBZ is an excellent inhibitor of C38 in the 1 M HCl medium.

3.2.2 Nyquist Impedance Diagram (EIS)

The Nyquist plots for C38 in 1 M HCl medium in presence and absence of OSBZ inhibitor at different concentrations are presented in Fig. 3. The impedance parameters are given in Table 4.

The inhibition efficiency of an organic compound is determined by the following relationship (Eq. 11):

$$\mathrm{IE}(\%) = \frac{R_{\mathrm{ct}}^{-1} - R_{\mathrm{ctinh}}^{-1}}{R_{\mathrm{ct}}^{-1}} \times 100, \tag{11}$$

where R_{ct}^{-1} and R_{ctinh}^{-1} are the charge transfer resistance respectively in the absence and in the presence of the inhibitor.

From Fig. 3, it is notice able that the impedance lines have a similar shape in all concentrations tested, indicating

Table 3 Electrochemical indices and IE (%) of MS in 1 M HCl at 298 K without and with addition of OSBZ at different concentrations

Concentration (M)	E_{corr}(mV/SCE)	β_c(mV/dec)	β_a(mV/dec)	I_{corr}(μA/cm²)	IE(%)
Blank	− 479.68	− 93.33	129.10	501.19	–
5×10^{-5}	− 462.74	− 80.77	135.45	151.38	69.80
10^{-4}	− 497.61	− 90.00	126.25	120.20	76.02
2×10^{-4}	− 481.53	− 74.35	112.31	85.11	83.02
3×10^{-4}	− 487.69	− 76.25	122.22	75.86	84.86

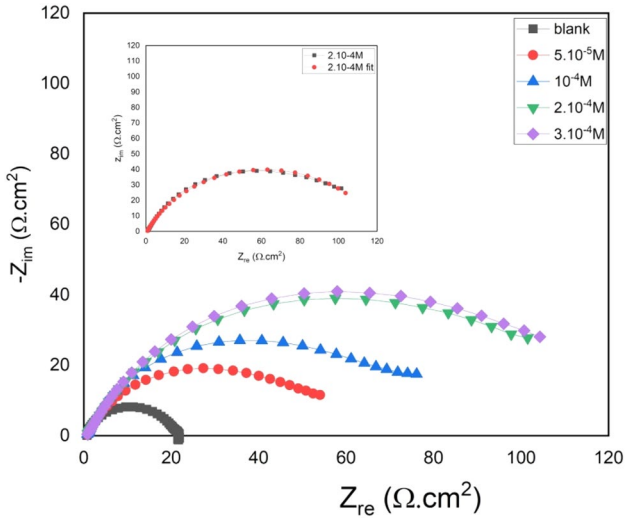

Fig. 3 Impedance diagrams of MS in 1 M HCl without and with addition of OSBZ at different concentrations at 298 K

that almost no change in the corrosion mechanism occurs due to the addition of inhibitor [47] also the loops are not standard semicircles at high frequencies generally attributed to the frequency dispersion which can be correlated with roughness, and heterogeneity of the metal surface such as impurities, grains boundaries, adsorption of the inhibitor and formation of porous layers [48, 49]. The equivalent circuit used to fit the experimental impedance data is represented in Fig. 4. This circuit consists of an electrolyte resistance (R_s) related in series with a constant phase elements (CPE) for double layer capacitance (C_{dl}) in parallel with a charge transfer resistance (R_{ct}).

The CPE was calculated by the following equation (Eq. 12) [50]:

$$\mathrm{ZCPE} = Q^{-1}(iw)^{-n}. \tag{12}$$

Q represent a factor of proportionality designate the greatness of CPE, i is the imaginary number, w is the angular frequency, and the exposant n is interlinked to the heterogeneity of the surface of metal, in the case of an ideal capacitor ($n=1$) and for a CPE ($n<1$) [50, 51].

The double layer capacitance (C_{dl}) is calculated by Eq. (13)

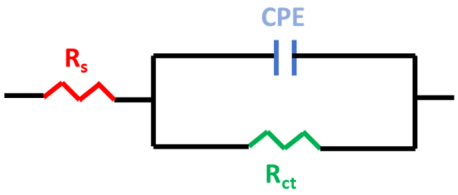

Fig. 4 Equivalent circuit for MS in 1 M HCl with addition of OSBZ at different concentrations at 298 K

$$C_{\mathrm{di}} = \left(QR_{\mathrm{ct}}^{1-n}\right)1/n, \tag{13}$$

where R_{ct} is the charge transfer resistance.

Table 4 shows that the values of charge transfer resistance R_{ct} increase with increasing concentration of the OSBZ compound, hence the increasing of the inhibition efficiency, suggesting the adsorption of OSBZ molecules at the metal surface [52]. In the other hand and in general, the estimated values of C_{dl} proves a decrease in the presence of OSBZ compound, indicate the formation of a protective film on the surface of the metal C38, and thus the OSBZ inhibitor replace the H_2O molecules present on the metal/solution interface. This decrement in the capacitance C_{dl} can be attributed to a lessening in the local dielectric constant or be referred to an elevation of the impact of electrostatic interaction [53].

The best inhibition efficiency calculated by this measurement was 83.16% at 3×10^{-4} M dose, which proves an excellent inhibition of the product studies. It is clear that there is a good agreement between this result and that obtained by the method of polarization curves; we also note that it is close to that of the mass loss measurement.

3.3 Adsorption Isotherm

The electrochemical reaction is done with a certain mechanism, to describe it, it is necessary to study the isotherm of adsorption [54]. There are many factors influencing the adsorption process such as temperature, surface characteristics of the metal, as well as the electronic properties of the inhibitor which are related to its structure [55].

Indeed to approach the adsorption mechanism of OSBZ on the surface of C38 we tried different adsorption isotherms, based on the results obtained through the PDP

Table 4 Electrochemical indices and IE (%) of MS in 1 M HCl without and with addition of OSBZ at different concentrations (at 298 K)

Concentration (M)	R_{ct} (Ωcm^2)	R_s (Ωcm^2)	C_{dl} (μF/cm^2)	Q(SW^{-1}/cm^2.10^{-4})	n	IE(%)
Blank	20.83	0.6937	384.70	7.597	0.859	–
5×10^{-5}	57.18	0.6988	258.50	6.895	0.7672	63.57
10^{-4}	77.95	0.6836	158.10	3.973	0.7904	73.28
2×10^{-4}	121.70	0.7454	248.80	6.214	0.7383	82.88
3×10^{-4}	123.70	0.7278	245.50	5.811	0.7534	83.16

study. It was found that the Langmuir's isotherm presents the best fit. This implies that the adsorption of inhibitor molecules on the surface of the metal is monolayer.

The Langmuir isotherm is the first choice for most models of adsorption and has many applications in surface kinetics.

The equation of this adsorption isotherm is [56]:

$$\frac{C_{\text{inh}}}{\theta} = \frac{1}{K_{\text{ads}}} + C_{\text{inh}}. \tag{14}$$

θ is the fraction of the surface sites covered, can be determined as follows (Eq. 15):

$$\theta = \frac{I_{\text{corr}(\theta=0)} - I_{\text{corr}(\theta)}}{I_{\text{corr}(\theta=0)} - I_{\text{corr}(\theta=1)}}, \tag{15}$$

where $I_{\text{corr}(\theta=0)}$ and $I_{\text{corr}(\theta)}$ are the corrosion current density in the absence and in the presence of the inhibitor at different concentrations, respectively.

$I_{\text{corr}(\theta=1)}$ is the corrosion current density in the presence of the inhibitor at optimum concentration. C_{inh} is the concentration of the inhibitor in the solution, K_{ads} is the equilibrium constant OSBZ adsorption–desorption processes.

The free energy of adsorption can be defined by the following relation (Eq. 16) [57]:

$$\Delta G^{\circ} = -RT\text{Ln}\left(55.55 \times K_{\text{ads}}\right), \tag{16}$$

where R is the universal gas constant ($R = 8.314$ J/mol/K), T is the temperature (K), and 55.55 value represent the molar concentration of water (mol/L).

The Langmuir plots ($\frac{C_{\text{inh}}}{\theta} = f\,(C_{\text{inh}})$) is illustrated in Fig. 5. It is clear that the curve as a straight line with a value of linear regression factor (R^2) closer to 1 (0.999). The calculated free energy value is − 37.62 kJ/mol.

In the one hand, this value is negative means that the interaction between the OSBZ inhibitor molecule and the surface of the C38 metal is strong, also indicating that this adsorption is done automatically [58]. In the other hand, the free energy value can tell us about the kind of adsorption of this inhibitor on the metal surface. Indeed, if the value of the free energy ΔG° in the domain of, or higher than − 20 kJ/mol means that there is an electrostatic interaction between the charged inhibitor molecules and the charged metal, it is a physisorption [59], and if ΔG° value in the horizon lower than − 40 kJ/mol indicates that there is a formation of a coordinate bond, the inhibitor shares charge with the metal surface, it is a chemisorption [60, 61]. In our case $\Delta G^{\circ} = -37.62$ kJ/mol proves that our OSBZ inhibitor adsorbs on the surface of the C38 metal according to the two mechanisms chemisorption and physisorption [62].

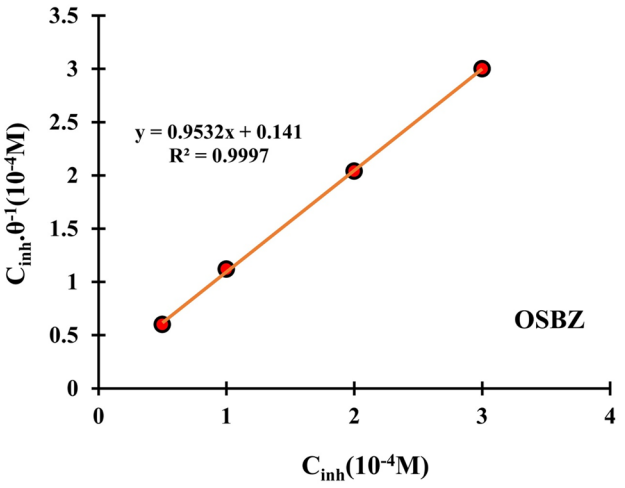

Fig. 5 Langmuir adsorption isotherm of OSBZ compound on the C38 at 298 K

3.4 Temperature Effect

The temperature of the corrosive medium is a main parameter which acts on the phenomenon of corrosion, the study of this effect can inform us about the mechanism of adsorption of the inhibitor and as well as the determination of the thermodynamic parameters. Figures 6 and 7 successively show the polarization curves of C38 in the absence and presence of OSBZ at 2×10^{-4} M (at different temperatures) the electrochemical parameters are presented in Tables 5 and 6.

It is clear that the gain in the current density within creasing temperature in the absence and in the presence of the OSBZ inhibitor, Hence the decrease in inhibition efficiency as a function of increasing temperature, which confirms that the increase in temperature induces an increase in the dissolution of the metal C38. This dissolution can be explained by a desorption or/and decomposition of the OSBZ inhibitor molecules.

3.5 Thermodynamic and Activation Parameters

The following equations (Eqs. 17–18) present the thermodynamic parameters.

$$\text{Arrhenius law}: I_{\text{corr}} = A\exp\left(-\frac{E_{\text{a}}}{R.T}\right), \tag{17}$$

$$\ln\left(I_{\text{corr}}\right) = \ln(A) - \frac{E_{\text{a}}}{R.T},$$

$$\text{Equation Arrhenius}: I_{\text{corr}} = \frac{K_{\text{B}}T}{h}\exp\left(\frac{\Delta S^{*}}{R}\right)\exp\left(-\frac{\Delta H^{*}}{R.T}\right), \tag{18}$$

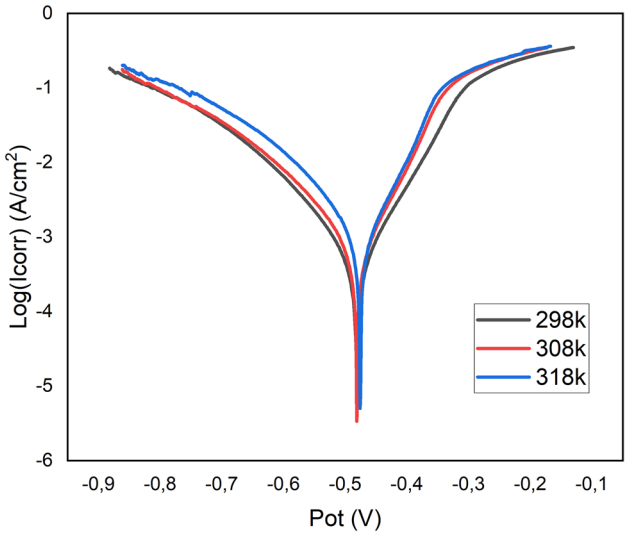

Fig. 6 Effect of temperature on steel polarization curves in 1 M HCl

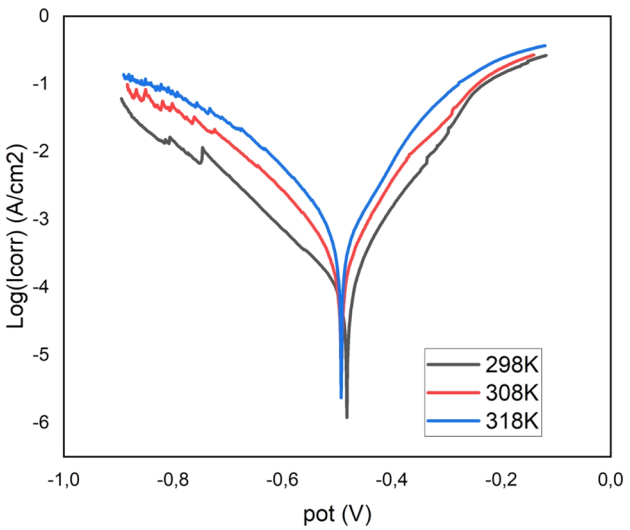

Fig. 7 Effect of temperature on steel polarization curves in 1 M HCl + OSBZ 2×10^{-4} M

$$\ln\left(\frac{I_{corr}}{T}\right) = A - \frac{\Delta H^*}{R.T},$$

Table 5 Effect of temperature on the electrochemical parameters of steel in 1 M HCl

Temperature (°C)	E_{corr} (mV/ECS)	β_c (mV/dec)	I_{corr} (µA/cm^2)
25	−479.68	−93.33	510.19
35	−478.87	−74.78	954.99
45	−477.13	−72.96	1698.24

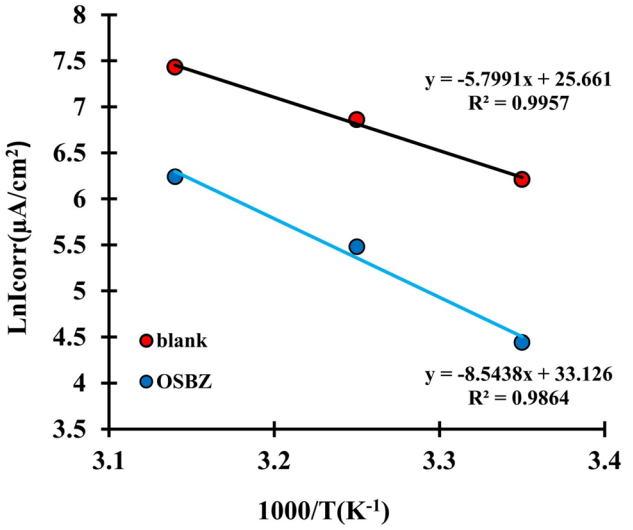

Fig. 8 The relationship between Ln(I_{corr}) as a function of 1/T of C38 in 1 M HCl without and with 2×10^{-4} M in OSBZ

Table 7 The corrosion activation energies of C38 in 1 M HCl without and with 2×10^{-4} M in OSBZ

Corrosive solution	Activation energy (kJ/mol)
HCl 1 M	48.20
HCl 1 M + 2×10^{-4} M OSBZ	71.00

where I_{corr} the corrosion current density, T the absolute temperature, E_a the activation energy, ΔH^* enthalpy, ΔS^* entropy, R (R = 8,314 J/mol/K) is the universal gas constant, K_B ($K_B = 1.38066\times10^{-23}$ J/K)is the Boltzmann constant, h ($h = 6.62\times10^{-34}$ J s) is the Plank constant.

Figure 8 shows the variation of Ln (I_{corr}) as a function of 1000/T of C38 in 1 M HCl with and without 2×10^{-4} M of OSBZ. These curves are linear which proves the verification of the Arrhenius law with a good correlation coefficient R^2. The activation energy was calculated from the slope ($-E_a/R$). The results are presented in Table 7.

Figure 9 shows the variation of Ln (I_{corr}/T) as a function of 1000/T of C38 in 1 M HCl with and without 2×10^{-4} M of OSBZ, these curves are linear. The slope is $-\frac{\Delta H^*}{R}$ and the ordinate at origin is $\mathrm{Ln}\frac{K_B}{h} + \left(\frac{\Delta S^*}{R}\right)$, from where the enthalpy

Table 6 Effect of temperature on the electrochemical parameters of steel in 1 M HCl + OSBZ 2×10^{-4} M

Temperature (°C)	E_{corr} (mV/ECS)	β_c(mV/dec)	I_{corr} (µA/cm^2)	η (%)
25	−481.53	−74.35	85.11	83.02
35	−491.59	−110	239.88	74.88
45	−490.13	−96	575.43	66.12

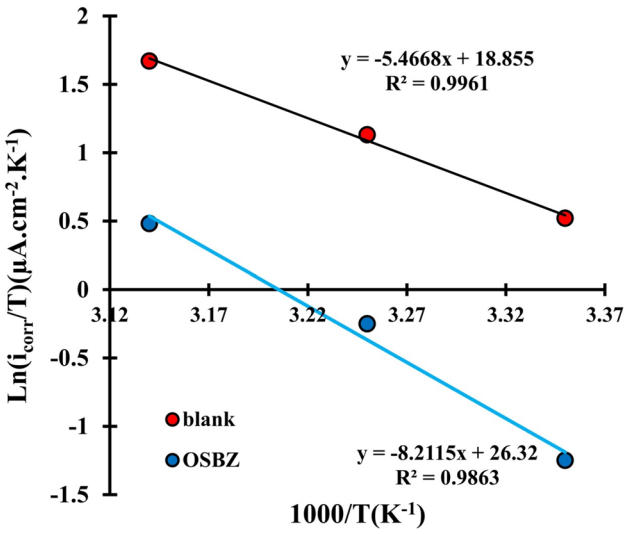

Fig. 9 The relationship between $\mathrm{Ln}(I_{corr}/T)$ as a function of $1/T$ of C38 in 1 M HCl without and with 2×10^{-4} M in OSBZ

Table 8 The corrosion activation parameters of C38 in 1 M HCl without and with 2×10^{-4} M in OSBZ

Medium	ΔH^* (kJ/mol)	ΔS^* (J/mol/K)	E_a (kJ/mol)	$E_a - RT$
Blank	45.40	−40.40	48.20	45.60
2×10^{-4}	68.30	21.70	71.00	68.40

ΔH^* as well as the entropy ΔS^* according to the results presented in Table 8, we observe that the activation energy in the presence of the OSBZ inhibitor is superior to that of white which means that OSBZ is an excellent inhibitor. This increase in activation energy indicates that the presence of the inhibitor OSBZ in the medium causes a slowdown in the process of corrosion of the metal C38 which is explained by the formation of an energy barrier without influencing the mechanism of dissolution of the metal [63, 64].

The values of ΔH^* taken from Fig. 9 are positive which shows that the process of the metal dissolution reaction is endothermic [65]. According to Table 8, the entropy value ΔS^* in the presence of OSBZ inhibitor is greater than in its absence, which means an increase in the disorder occurring between the steps from the reactants to the formation of the activated complex.

This increase in the entropy ΔS^* which is due to the adsorption of inhibitor molecules on the surface of C38 metal could be estimated as a quasi-substitution between the inhibitor molecules in the aqueous phase and the H_2O molecules located on the surface electrodes [48]. Therefore the adsorption of OSBZ molecules obeys desorption of H_2O molecules from the surface of the electrode and subsequently deceases the electrical capacity of the metal.

We also note that the activation energies E_a higher than the analogous values of the enthalpy ΔH^* indicating that the corrosion process includes a gaseous reaction it is the formation of H_2, moreover the difference of $(E_a - RT)$ is close to the value of ΔH^* where the temperature T is between 298 and 318 K, expressing that the corrosion process is a unimolecular reaction [66].

3.6 Surface Analysis

3.6.1 SEM Analysis

The morphology of the studied surface has been analyzed by the scanning electron microscope (SEM) technique. This examination is carried out before and after immersion of samples in the corrosive medium without and with inhibitor. The corresponding images are grouped together. In Fig. 10A of the blank sample is characterized by simple scratches due to abrasion. Moreover, the image (B) which represents the metal immersed in the HCl medium (1 M) is very corroded by several deepits. On the other hand, image C of sample C38 after immersion in the medium (HCl + OSBZ) shows that there is a remarkable improvement in the surface of the metal, which is more protected by the formation of a protective layer in the presence of OSBZ.

3.6.2 EDS Analysis

The observations made by the image (SEM) are confirmed by the technique of energy dispersive X-ray spectrometry (EDS), according to the spectra mentioned in Fig. 11A, B represent successively the sample of the abraded steel and the one immersed in the 1 M HCl solution and also the results of Table 9, it is noticed that there is a decrease in the percentage of iron (98.70%/75.47%). This is explained by the transfer of iron in hydrochloric acid solution. On the other hand the spectra represented in image C corresponds to the metal immersed in the medium (HCl + OSBZ) as well as Table 9 shows a decrease in the corrosion rate. This is illustrated by the increase in the percentage of iron (96.70%) and a remarkable decrease in the percentage of oxygen (14.60% in HCl alone/0.86% in HCl + OSBZ) which implies a decrease in the formation of iron oxide, thus fighting against corrosion. This proves that the OSBZ compound is a good inhibitor for this steel in the 1 M HCl medium.

3.7 Quantum Chemical Calculations

3.7.1 Global Reactivity

Figure 12 represent the geometrical structure of the inhibitor molecule in the neutral state in aqueous phase are obtained by a global optimization characterized by a calculation of

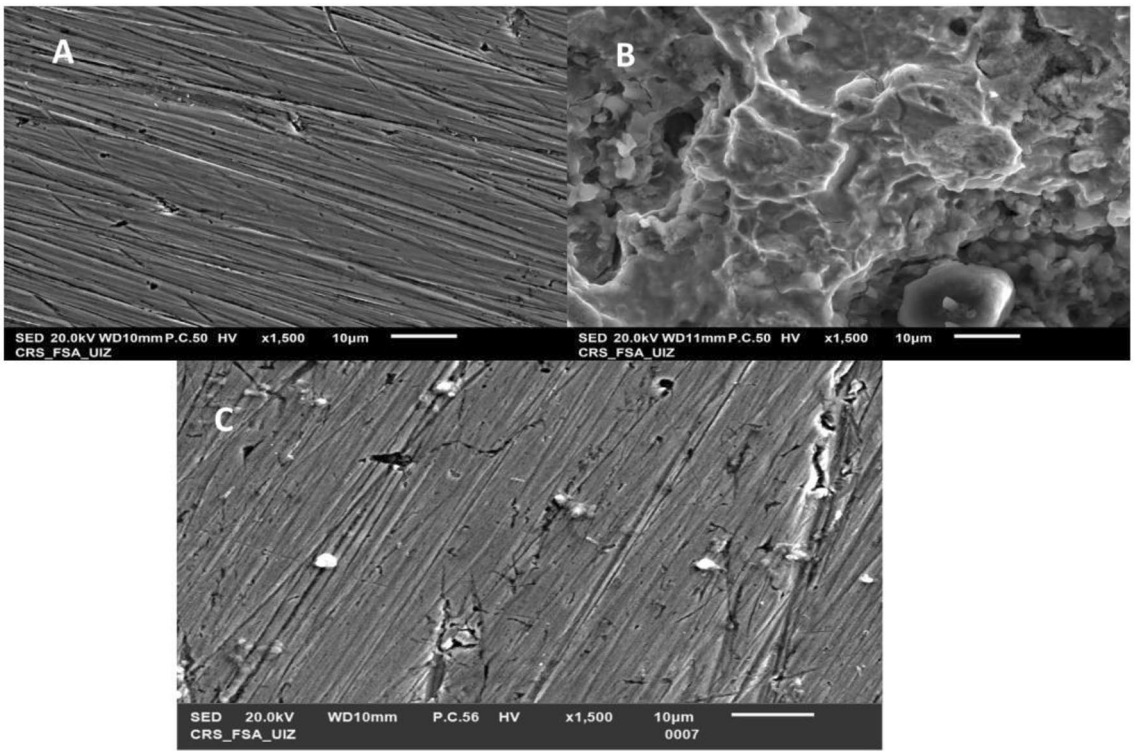

Fig. 10 SEM micrographs of **A** polished sample, **B**, the sample in 1 M HCl, and **C** the sample in 1 M HCl in the presence of OSBZ

the vibration frequencies using DFT B3LYP/6-311G (p,d) level in the neutral phase.

It is well established in the literature that conjugated compounds containing heteroatoms such as nitrogen, oxygen, sulfur or phosphorus in their molecular structures are often very good corrosion inhibitors [67].

Indeed, this compound can adsorbs on iron surface by the double boundary π, blocking active sits and slowing corrosion rates. A number of studies haves how that nitrogen-containing heterocyclic compounds remain excellent inhibitors of iron surface in corrosive environments [68].

It can be seen that the electron density of the HOMO and LUMO location has been distributed almost on the whole molecule, due to the presence of nitrogen atoms, oxygen and carbon atoms with several electrons π and *n* in the chemical structure of OSBZ. Moreover, electrons from the inhibitor molecule can be taken up by the iron atom's empty (d) orbital to create a coordination bung. Additionally, the inhibitor molecule's anti-bonding orbitals can receive electrons from the iron atom to create a binding bung back [69]. Which can be useful for the adsorption mechanism of the inhibitor on the iron surface.

The DFT parameters of neutral forms of OSBZ are given in Table 10.

The result in Table 10: demonstrate that OSBZ has a low value for the energy gap (E_{GAP}) between E_{HOMO} and E_{LUMO}, a high value for the HOMO energy, and a high value for the LUMO energy, all of which increase its inhibitory influence on the surface of the iron [70].

A molecule's dipole moment is the factor that is most frequently employed to characterize its polarity. It is the measure of the polarity of a dipolar covalent bond. It is defined as the product of charge in the atom and the distance between two polar covalent bonds [71]. However, the total dipole moment just reflects the overall polarity of the molecule.

The literature has conclusively demonstrated that molecules with higher dipole moments are more reactive. The dipole moment in our investigation has a value of 94.050 Debye [72].

3.7.2 Local Molecular Reactivity

Inhibitor molecules interact with metallic surfaces in a donor–acceptor manner to adsorb on them. Analyzing which atoms in the molecules mostly participate in this donor-accepter sort of interaction is therefore, crucial. We learned in general if inhibitor compounds are able to give and take electrons from the preceding discussion (the section on quantum chemical calculations) [73] However, it is crucial to locate the matching active sites that are in charge of this electron donation and acceptance. A useful approach for determining the local active regions of an inhibitory chemical is called local reactivity [74]. For OSBZ, the estimated Fukui indices of simplified functions

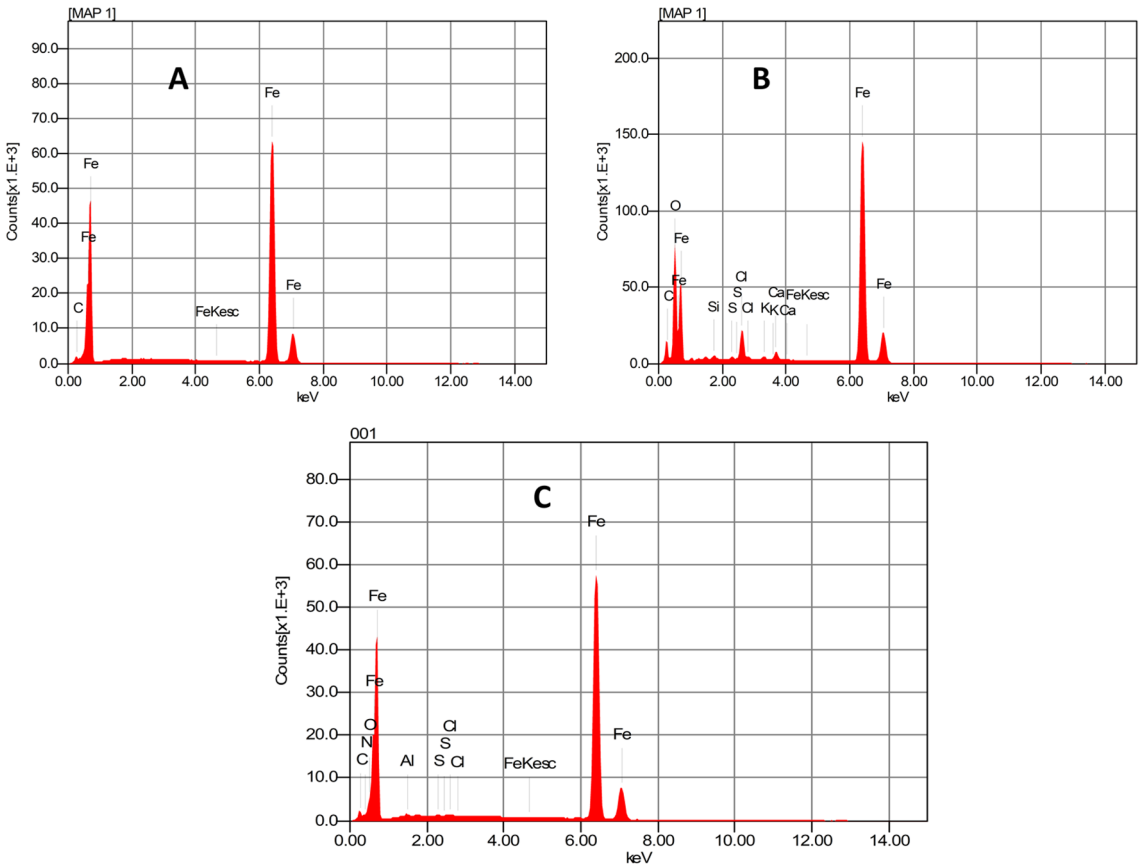

Fig. 11 EDS spectra of **A** polished sample, **B**, the sample in 1 M HCl, and **C** the sample in 1 M HCl in the presence of OSBZ

Table 9 Elementary composition of different sample of C38 with and without OSBZ inhibitor

Sample condition	Fe	O
The sample polished	98.70	0.00
The sample in 1 M HCl	75.47	14.16
The sample in 1 M HCl + OSBZ	96.96	0.86

(f^+ and f^-) are shown in Figs. 13 and 14 In contrast to the active centers used in nucleophilic attacks, which have a greater f^+ value, electrophilic attacks' active centers have a higher f^- value [75]. The results demonstrate that the C(2) and C(5) atoms were involved in electrophilic assaults, demonstrating its propensity to contribute electrons to the formation of more stable coordination bonds with the metal surface. During nucleophilic assaults, atoms like C(17) and C(29) can accept electrons from the metal surface. These findings imply that these locations local responsiveness to participating in.

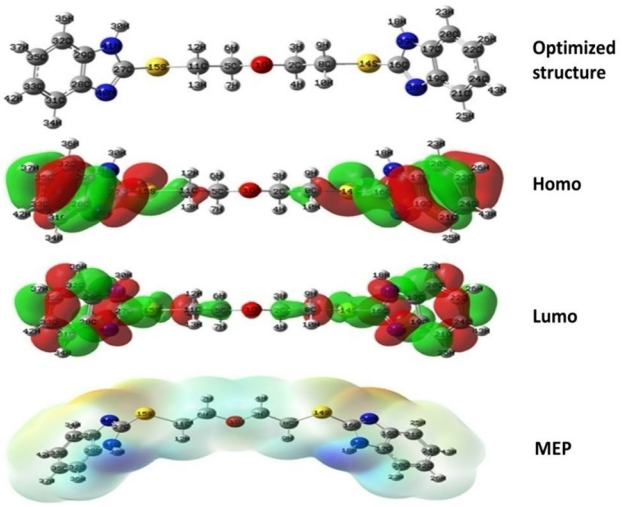

Fig. 12 Geometry-optimized structures, HOMO, LUMO orbitals, and MEP of OSBZ at the DFT B3LYP/6-311G (p,d) level in the neutral phase

Table 10 DFT parameters in eV of neutral forms of OSBZ

Inhibitor	E_{LUMO} (eV)	E_{HOMO} (eV)	ΔE (eV)	η (eV)	σ (eV^{-1})	χ (eV)	ω (eV)	ΔN	Dipole moment (Debye)
OSBZ	− 1.3456	− 6.6338	5.2882	2.6441	0.3781	3.9897	3.010	0.1570	94.050

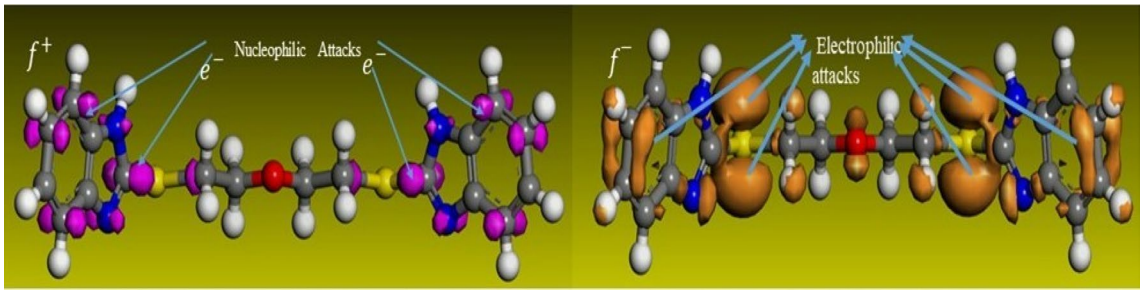

Fig. 13 Fukui functions condensed on f^+ and f^- atoms of OSBZ estimated by DFT/GGA/DNP using Materials Studio software

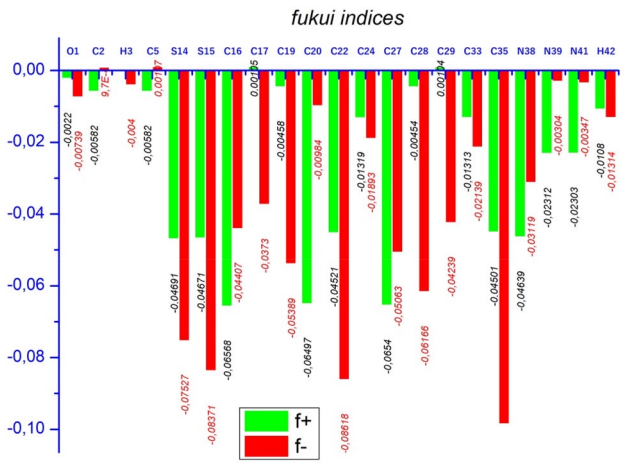

Fig. 14 Graphical graph of the Fukui indices for OSBZ

3.8 Molecular Dynamics Simulations MDs

To investigate and understand the interactions between inhibitor molecules and the surface of carbon steel, MD simulations are frequently performed. In this section, the interaction system has been modeled in both the absence of the solvent molecules (H_2O) and the presence of the solvent molecules [76].

The molecular structure of the inhibitor reveals that the development of coordination bonds between iron and the aromatic cycles included in the inhibitor and adsorption on the surface of carbon-containing metals are made possible by sharing the azote's electrons. On the other hand, the attraction of the surface of the net molecule may be influenced by the physical contacts between the inhibitor molecules and the metal surface, caused by Van Der Waals dispersion forces [77]. The strong contact between the two aromatic rings of the investigated molecule and the metal surface is responsible for this method of adsorption. As was already established, the iron's vacant d orbital can accept electrons from the nitrogen atoms in the inhibitor molecule to create coordination bonds [78]. Figure 15 shows a parallel adsorption of the molecule OSBZ in both aqueous and vacuum medium, wish mean the efficient adoption mode the de OSBZ inhibitor. Moreover the distance between iron surface and OSBZ inhibitor (3.18 A) are smaller in aqueous medium than the vacuum medium (3.8 A) wish indicate the water molecules increase the binding interactions between iron surface and OSBZ molecules.

In this part, we estimated the interaction and binding energies between the molecule under investigation and iron in both the presence and absence of the solvent (H_2O), and the findings are organized in Table 11. The iron atoms and inhibitor molecules' negative interaction energies − 603.347 kJ/mol and − 796.956 kJ/mol indicate the spontaneity of the adsorption process [79]. A more persistent inhibitor/surface contact results from an inhibitor molecule's highest binding energy and most negative interaction energy [79].

4 Conclusion

The inhibitory activity of MS type C38 in acidic medium of 1 M HCl of a new synthesized compound 1,5-bis-2-[benzimidazol-2-yl]mercaptodiethyleneglycol of benzimidazole type was studied, it was found that the latter is a good inhibitor which is in agreement with the literature that states that benzimidazoles are better inhibitors of MSs to different acidic media.

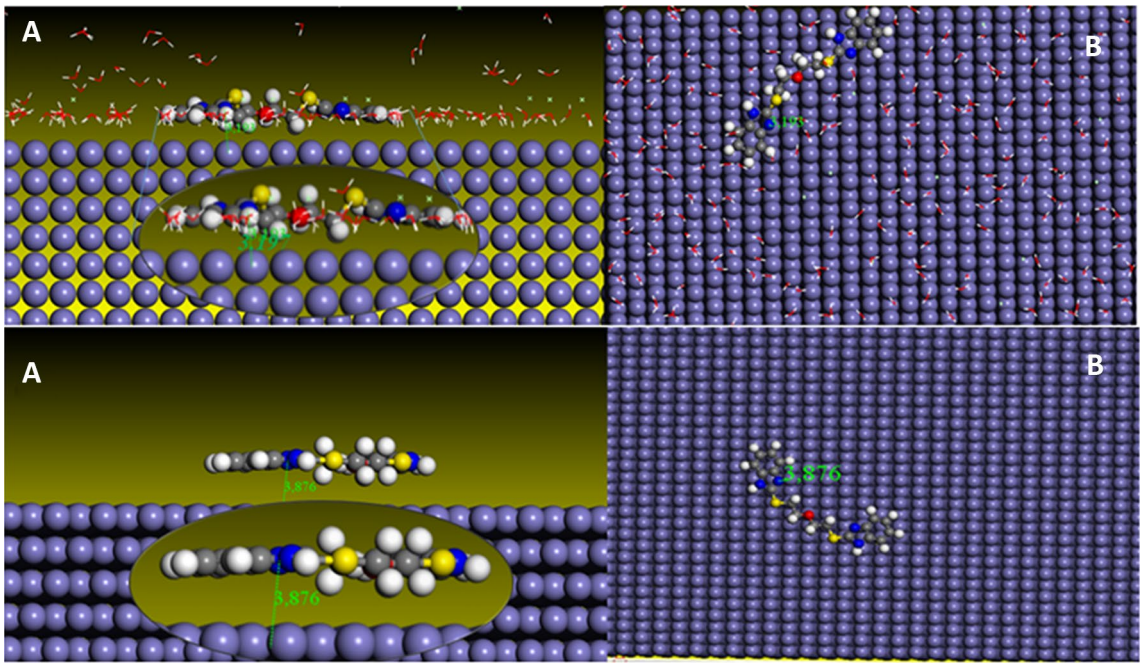

Fig. 15 The inhibitor molecule in equilibrium adsorption configurations on the surface of Fe (110): **A** without solvent and **B** with water. Right: a side view; left: a top view

Table 11 The interaction and binding energies between the OSBZ inhibitor molecule and the surface of Fe (110)

Systems	$E_{\text{Interaction}}$ (kJ mol^{-1})	E_{binding} (kJ/mol)
Fe + OSBZ	− 603.347	603.347
Fe + OSBZ + water	− 796.956	796.956

Experimental studies show that:

- The gravimetric study showed that the OSBZ compound protected the C38 metal surface in 1 M HCl which is confirmed by the decrease of the corrosion rate.
- From the polarization method it could be concluded that the OSBZ compound is a good inhibitor of the studied steel due to the decrease of the corrosion density.
- The gravimetric and electrochemical study showed that the efficiency increases with the increase of the concentration of the OSBZ compound in the corrosive environment (to reach a neighborhood of 90%).
- And from the study of the effect of temperature it was found that the inhibitory efficiency decreases with increasing temperature.
- It was deduced that the adsorption isotherm is obeying the Langmuir model and the value of free energy informed us that the inhibitor adsorbs on the surface with both chemisorption and physisorption mechanisms.
- The analysis of polarization curves at different concentrations of OSBZ inhibitor showed that this inhibitor is of mixed cathodic and anodic type with a cathodic predominance. The discharge of the proton H^+ on the surface of the steel is done according to a mechanism pure activation, also the hydrogen reduction mechanism is not affected by OSBZ.
- The results from the impedance curves reported a decrease in the double layer capacitance which is justified by the adsorption of the OSBZ molecules on the metal surface resulting in the formation of a protective layer.
- SEM pictures showed that the surface of the metal immersed in the solution containing OSBZ compound is less corroded rather more uniform than the one immersed in the corrosive medium without OSBZ, this proves that the inhibitor molecules are adsorbed on the surface of the metal to form a protective layer. These results are confirmed by EDS analysis where the percentage of iron on the metal surface is increased in the presence of the inhibitor but the percentage of oxygen is decreased, thus forming a protective barrier which is in agreement with the previous results.

Theatrical studies show that:

- Corrosion inhibitory efficiency increases with higher values of E_{HOMO}, μ, σ and ΔN and lower values of ΔE_{GAP}, E_{LUMO}, ω and η.

- The principal adsorption centers include S, N, and O as well as the aromatic rings found in the inhibitor's molecular structure, according to the predicted areas of molecular electrostatic potential.
- The results of MD simulations indicate that the inhibitor is adsorbed in a quasi-parallel mode with respect to the metal surface, which confirms the strong interaction between the inhibitor and the iron atoms. On the other hand, in an aqueous solution the inhibitor adsorbed by the Fe (110) surface is oriented almost horizontally. In addition, the most negative adsorption energy and high binding energy values led to more stable inhibitor/surface interactions;
- It is concluded that quantum chemical calculations and MD simulations are in perfect harmony with the experimental study.

Author Contributions NJ experimental and theoretical studies, wrote the main manuscript, HEE and HE supervision and correction of the manuscript, HAS and SJ molecule synthesis, AM theoretical study, MH and MMR direction of the experimental study. All authors reviewed the manuscript.

Funding This research did not receive any specific grant from funding agencies in the public, commercial, or not-for-profit sectors.

Data Availability All the data used in the investigation are available in the manuscript, the Supplementary Data that support the findings of this study are available to the corresponding author.

Declarations

Conflict of interest On behalf of all authors, the corresponding author states that there is no conflict of interest.

Ethical Approval Not applicable.

Informed Consent Not applicable.

Consent for Publication The authors hereby consent to publication of the work in this journal.

References

1. Fajobi MA, Fayomi OSI, Akande IG, Odunlami OA (2019) Inhibitive performance of ibuprofen drug on mild steel in 0.5 M of H2SO4 acid. J Bio Tribo-Corros 5(3):79. https://doi.org/10.1007/s40735-019-0271-3
2. El Maraghi A, El Alaoui El Abdallaoui H, Garmes G, Byadi S (2023) Corrosion inhibition by indazole derivatives in 1 M HCl medium: experimental and computational studies. J Bio Tribo-Corros 9(1):15. https://doi.org/10.1007/s40735-022-00731-8
3. de la Fuente D, Díaz I, Simancas J, Chico B, Morcillo M (2011) Long-term atmospheric corrosion of mild steel. Corros Sci 53(2):604–617. https://doi.org/10.1016/j.corsci.2010.10.007
4. Asegbeloyin J, Ejikeme P, Olasunkanmi L, Adekunle A, Ebenso E (2015) A novel Schiff base of 3-acetyl-4-hydroxy-6-methyl-(2*H*)pyran-2-one and 2, 2′-(ethylenedioxy)diethylamine as potential corrosion inhibitor for mild steel in acidic medium. Materials 8(6):2918–2934. https://doi.org/10.3390/ma8062918
5. Mashuga M, Olasunkanmi L, Adekunle A, Yesudass S, Kabanda M, Ebenso E (2015) Adsorption, thermodynamic and quantum chemical studies of 1-hexyl-3-methylimidazolium based ionic liquids as corrosion inhibitors for mild steel in HCl. Materials 8(6):3607–3632. https://doi.org/10.3390/ma8063607
6. Gutiérrez E, Rodríguez JA, Cruz-Borbolla J, Alvarado-Rodríguez JG, Thangarasu P (2016) Development of a predictive model for corrosion inhibition of carbon steel by imidazole and benzimidazole derivatives. Corros Sci 108:23–35. https://doi.org/10.1016/j.corsci.2016.02.036
7. AhadiParsa M, Dehghani A, Ramezanzadeh M, Ramezanzadeh B (2022) Rising of MXenes: novel 2D-functionalized nanomaterials as a new milestone in corrosion science—a critical review. Adv Colloid Interface Sci 307:102730. https://doi.org/10.1016/j.cis.2022.102730
8. Ani JU, Obi IO, Akpomie KG, Eze SI, Nwatu G (2022) Corrosion inhibition studies of metals in acid media by fibrous plant biomass extracts and density functional theory: a mini-review. J Nat Fibers 19(7):2391–2401. https://doi.org/10.1080/15440478.2020.1818345
9. Finšgar M, Jackson J (2014) Application of corrosion inhibitors for steels in acidic media for the oil and gas industry: a review. Corros Sci 86:17–41. https://doi.org/10.1016/j.corsci.2014.04.044
10. Singh A et al (2018) Effect of electron donating functional groups on corrosion inhibition of mild steel in hydrochloric acid: experimental and quantum chemical study. J Taiwan Inst Chem Eng 82:233–251. https://doi.org/10.1016/j.jtice.2017.09.021
11. Onyeachu IB, Obot IB, Sorour AA, Abdul-Rashid MI (2019) Green corrosion inhibitor for oilfield application I: electrochemical assessment of 2-(2-pyridyl) benzimidazole for API X60 steel under sweet environment in NACE brine ID196. Corros Sci 150:183–193. https://doi.org/10.1016/j.corsci.2019.02.010
12. Aljourani J, Golozar MA, Raeissi K (2010) The inhibition of carbon steel corrosion in hydrochloric and sulfuric acid media using some benzimidazole derivatives. Mater Chem Phys 121(1–2):320–325. https://doi.org/10.1016/j.matchemphys.2010.01.040
13. Chacko M, Nayak J (2015) Benzimidazole as corrosion inhibitor for heat treated 6061 Al–SiC_p composite in acetic acid. J Phys Conf Ser 622:012035. https://doi.org/10.1088/1742-6596/622/1/012035
14. Shanbhag AV, Venkatesha TV, Praveen BM (2013) Benzimidazole derivatives as corrosion inhibitors for zinc in acid solution. Prot Met Phys Chem Surf 49(5):4
15. Garcia-Ochoa E, Guzmán-Jiménez SJ, Hernández JG, Pandiyan T, Vásquez-Pérez JM, Cruz-Borbolla J (2016) Benzimidazole ligands in the corrosion inhibition for carbon steel in acid medium: DFT study of its interaction on Fe_{30} surface. J Mol Struct 1119:314–324. https://doi.org/10.1016/j.molstruc.2016.04.057
16. Khaled KF (2003) The inhibition of benzimidazole derivatives on corrosion of iron in 1 M HCl solutions. Electrochim Acta 48(17):2493–2503. https://doi.org/10.1016/S0013-4686(03)00291-3
17. Bereket G, Pınarbaşı A, Öğretir C (2004) Benzimidazole-2-tione and benzoxazole-2-tione derivatives as corrosion inhibitors for aluminium in hydrochloric acid. Anti-Corros Methods Mater 51(4):282–293. https://doi.org/10.1108/00035590410541364
18. El-Hajjaji F et al (2019) 1-Octyl-2-(octylthio)-1*H*-benzimidazole as a new and effective corrosion inhibitor for carbon steel in 1 M

HCl. Port Electrochim Acta 37(3):131–145. https://doi.org/10.4152/pea.201903131
19. Rodriguez-Clemente E et al (2018) New 1-(2-pyridinyl)-2-(*o*-, *m*-, *p*-hydroxyphenyl) benzimidazoles as corrosion inhibitors for API 5L X52 steel in acid media. Anti-Corros Methods Mater 65(2):166–175. https://doi.org/10.1108/ACMM-06-2017-1811
20. Niamien PM, Kouassi HA, Trokourey A, Essy FK, Sissouma D, Bokra Y (2012) Copper corrosion inhibition in 1 M HNO_3 by two benzimidazole derivatives. ISRN Mater Sci 2012:1–15. https://doi.org/10.5402/2012/623754
21. Zhang D, Gao L, Zhou G (2004) Inhibition of copper corrosion in aerated hydrochloric acid solution by heterocyclic compounds containing a mercapto group. Corros Sci 46(12):3031–3040. https://doi.org/10.1016/j.corsci.2004.04.012
22. Dutta A, Saha SK, Adhikari U, Banerjee P, Sukul D (2017) Effect of substitution on corrosion inhibition properties of 2-(substituted phenyl) benzimidazole derivatives on mild steel in 1 M HCl solution: a combined experimental and theoretical approach. Corros Sci 123:256–266. https://doi.org/10.1016/j.corsci.2017.04.017
23. Dutta A, Saha SK, Banerjee P, Sukul D (2015) Correlating electronic structure with corrosion inhibition potentiality of some bis-benzimidazole derivatives for mild steel in hydrochloric acid: combined experimental and theoretical studies. Corros Sci 98:541–550. https://doi.org/10.1016/j.corsci.2015.05.065
24. Popova A, Sokolova E, Raicheva S, Christov M (2003) AC and DC study of the temperature effect on mild steel corrosion in acid media in the presence of benzimidazole derivatives. Corros Sci 45(1):33–58. https://doi.org/10.1016/S0010-938X(02)00072-0
25. Kenitra M, Lgaz H, Salghi R, Jodeh S (2016) Corrosion inhibition potentiality of some benzimidazole derivatives for mild steel in hydrochloric acid: electrochemical and weight loss studies. Int. J. Corros. Scale Inhib. 5(4):347–359. https://doi.org/10.17675/2305-6894-2016-5-4-5
26. Keri RS, Hiremathad A, Budagumpi S, Nagaraja BM (2015) Comprehensive review in current developments of benzimidazole-based medicinal chemistry. Chem Biol Drug Des 86(1):19–65. https://doi.org/10.1111/cbdd.12462
27. El-Kihel A et al (2019) Synthesis and anticancer activity of glycol-bridged bis-benzimidazoles. DJ J Eng Chem Fuel. https://doi.org/10.18831/djchem.org/2019011006
28. Salman TA et al (2019) Effect of 1, 3, 4-thiadiazole scaffold on the corrosion inhibition of mild steel in acidic medium: an experimental and computational study. J Bio Tribo-Corros 5(2):48. https://doi.org/10.1007/s40735-019-0243-7
29. El Asri A et al (2022) Computational and experimental studies of the inhibitory effect of imidazole derivatives for the corrosion of copper in an acid medium. J Mol Liq 345:117813. https://doi.org/10.1016/j.molliq.2021.117813
30. Shainy KM, Rugmini Ammal P, Unni KN, Benjamin S, Joseph A (2016) Surface interaction and corrosion inhibition of mild steel in hydrochloric acid using pyoverdine, an eco-friendly biomolecule. J Bio Tribo-Corros 2(3):20. https://doi.org/10.1007/s40735-016-0050-3
31. Boughoues Y, Benamira M, Messaadia L, Ribouh N (2020) Adsorption and corrosion inhibition performance of some environmental friendly organic inhibitors for mild steel in HCl solution via experimental and theoretical study. Colloids Surf A 593:124610. https://doi.org/10.1016/j.colsurfa.2020.124610
32. Sadik K, El Hamdani N, Byadi S, Hachim ME, El Harafi H, Aboulmouhajir A (2021) Quantum and dynamic investigations of Complex iron-alkaloid-extract Cytisine derivatives of *Retama monosperma* (L.) Boiss. Seeds as eco-friendly inhibitors for mild steel corrosion in 1 M HCl. J Mol Struct 1244:130921. https://doi.org/10.1016/j.molstruc.2021.130921
33. Abdelmalek M et al (2021) Corrosion inhibition performance of azelaic acid dihydrazide: a molecular dynamics and Monte Carlo simulation study. J Mol Model 27(11):331. https://doi.org/10.1007/s00894-021-04955-2
34. Wazzan N (2023) Phytochemical components of *Allium jesdianum* flower as effective corrosion-resistant materials for Fe(1 1 0), Al(1 1 1), and Cu(1 1 1): DFT study. Arab J Chem 16(4):104625. https://doi.org/10.1016/j.arabjc.2023.104625
35. Olasunkanmi LO, Obot IB, Kabanda MM, Ebenso EE (2015) Some quinoxalin-6-yl derivatives as corrosion inhibitors for mild steel in hydrochloric acid: experimental and theoretical studies. J Phys Chem C 119(28):16004–16019. https://doi.org/10.1021/acs.jpcc.5b03285
36. Faska Z, Majidi L (2018) DFT study on the adsorption mechanism of pulegone and pulegone oxide molecules in gas and aqueous phases as effective corrosion inhibitors in Molar Hydrochloric Acid. Moroc J Chem 6(2):11
37. Fakhry H et al (2022) Experimental, DFT studies and molecular dynamic simulation on the corrosion inhibition of carbon steel in 1 M HCl by two newly synthesized 8-hydroxyquinoline derivatives. J Indian Chem Soc. https://doi.org/10.1016/j.jics.2022.100701
38. Zhu Y, Sun Q, Wang Y, Tang J, Wang Y, Wang H (2021) Molecular dynamic simulation and experimental investigation on the synergistic mechanism and synergistic effect of oleic acid imidazoline and L-cysteine corrosion inhibitors. Corros Sci 185:109414. https://doi.org/10.1016/j.corsci.2021.109414
39. Kr S, Hens A (2014) Molecular dynamics and density functional theory study on corrosion inhibitory action of three substituted pyrazine derivatives on steel surface. Can Chem Trans. https://doi.org/10.13179/canchemtrans.2014.02.04.0137
40. About H et al (2018) Experimental and theoretical studies of 5-((4-phenyl-4,5-dihydro-1*H*-tetrazol-1-yl)methyl)-quinolin-8-ol quinoline derivative as effective corrosion inhibitor for mild steel 1.0 HCl. J Mater Environ Sci 9(1):345–357. https://doi.org/10.26872/jmes.2018.9.1.38
41. Ouakki M, Rbaa M, Galai M, Lakhrissi B, Rifi EH, Cherkaoui M (2018) Experimental and quantum chemical investigation of imidazole derivatives as corrosion inhibitors on mild steel in 1.0 M hydrochloric acid. J Bio Tribo-Corros 4(3):35. https://doi.org/10.1007/s40735-018-0151-2
42. Verma C, Olasunkanmi LO, Ebenso EE, Quraishi MA (2018) Substituents effect on corrosion inhibition performance of organic compounds in aggressive ionic solutions: a review. J Mol Liq 251:100–118. https://doi.org/10.1016/j.molliq.2017.12.055
43. Zhang W et al (2019) Tetrahydroacridines as corrosion inhibitor for X80 steel corrosion in simulated acidic oilfield water. J Mol Liq 293:111478. https://doi.org/10.1016/j.molliq.2019.111478
44. Yıldız R, Döner A, Doğan T, Dehri İ (2014) Experimental studies of 2-pyridinecarbonitrile as corrosion inhibitor for mild steel in hydrochloric acid solution. Corros Sci 82:125–132. https://doi.org/10.1016/j.corsci.2014.01.008
45. Yadav M, Behera D, Kumar S, Sinha RR (2013) Experimental and quantum chemical studies on the corrosion inhibition performance of benzimidazole derivatives for mild steel in HCl. Ind Eng Chem Res 52(19):6318–6328. https://doi.org/10.1021/ie400099q
46. Solmaz R (2014) Investigation of corrosion inhibition mechanism and stability of Vitamin B_1 on mild steel in 0.5 M HCl solution. Corros Sci 81:75–84. https://doi.org/10.1016/j.corsci.2013.12.006
47. Labjar N, Lebrini M, Bentiss F, Chihib N-E, Hajjaji SE, Jama C (2010) Corrosion inhibition of carbon steel and antibacterial properties of aminotris-(methylenephosphonic) acid. Mater Chem Phys 119(1–2):330–336. https://doi.org/10.1016/j.matchemphys.2009.09.006

48. Chakravarthy MP, Mohana KN (2014) Adsorption and corrosion inhibition characteristics of some nicotinamide derivatives on mild steel in hydrochloric acid solution. ISRN Corros 2014:1–13. https://doi.org/10.1155/2014/687276
49. Zarrouk A et al (2016) Inhibitive properties, adsorption and theoretical study of 3,7-dimethyl-1-(prop-2-yn-1-yl)quinoxalin-2(1*H*)-one as efficient corrosion inhibitor for carbon steel in hydrochloric acid solution. J Mol Liq 222:239–252. https://doi.org/10.1016/j.molliq.2016.07.046
50. Faydy ME et al (2019) Corrosion protection of carbon steel by two newly synthesized benzimidazol-2-ones substituted 8-hydroxyquinoline derivatives in 1 M HCl: experimental and theoretical study. Surf Interfaces 14:222–237. https://doi.org/10.1016/j.surfin.2019.01.005
51. Rguiti MM et al (2018) Iron corrosion inhibition by olive mill wastewaters in acid medium. Moroc J Chem 6(2):11
52. Solmaz R (2014) Investigation of adsorption and corrosion inhibition of mild steel in hydrochloric acid solution by 5-(4-dimethylaminobenzylidene)rhodanine. Corros Sci 79:169–176. https://doi.org/10.1016/j.corsci.2013.11.001
53. Kumar S et al (2022) Synthesis, characterization and anticorrosive effect of 2-(phenoxy methyl)-5-phenyl-1, 3, 4-oxadiazole for mild steel in 1 M HCl: a combined experimental and computational demonstrations. J Indian Chem Soc 99(5):100421. https://doi.org/10.1016/j.jics.2022.100421
54. Paul S, Koley I (2016) Corrosion inhibition of carbon steel in acidic environment by papaya seed as green inhibitor. J Bio Tribo-Corros 2(2):6. https://doi.org/10.1007/s40735-016-0035-2
55. El Ibrahimi B et al (2019) Effect of solution's pH and molecular structure of three linear α-amino acids on the corrosion of tin in salt solution: a combined experimental and theoretical approach. J Mol Struct 1196:105–118. https://doi.org/10.1016/j.molstruc.2019.06.072
56. Zarrouk A et al (2012) Some new ionic liquids derivatives: synthesis, characterization and comparative study towards corrosion of C-steel in acidic media. J Chem Pharm Res 4(7):11
57. Zarrok H et al (2012) Thermodynamic characterisation and density functional theory investigation of 1, 1′, 5, 5′-tetramethyl-1*H*, 1′*H*-3, 3′-bipyrazole as corrosion inhibitor of C38 steel corrosion in HCl. Int J Electrochem Sci 7:17
58. Chadili M et al (2021) Corrosion inhibition of 3003 aluminum alloy in molar hydrochloric acid solution by olive oil mill liquid by-product. Int J Corros 2021:1–13. https://doi.org/10.1155/2021/6662395
59. El Faydy M et al (2016) Experimental investigation on the corrosion inhibition of carbon steel by 5-(chloromethyl)-8-quinolinol hydrochloride in hydrochloric acid solution. J Mol Liq 219:396–404. https://doi.org/10.1016/j.molliq.2016.03.056
60. El Yaktini A et al (2018) Inhibitor effect of new azomethine derivative containing an 8-hydroxyquinoline moiety on corrosion behavior of mild carbon steel in acidic media. Int J Corros Scale Inhib. https://doi.org/10.17675/2305-6894-2018-7-4-9
61. Kumar R, Chopra R, Singh G (2017) Electrochemical, morphological and theoretical insights of a new environmentally benign organic inhibitor for mild steel corrosion in acidic media. J Mol Liq 241:9–19. https://doi.org/10.1016/j.molliq.2017.05.130
62. Sangeetha Y, Meenakshi S, Sairam Sundaram C (2016) Corrosion inhibition of aminated hydroxyl ethyl cellulose on mild steel in acidic condition. Carbohydr Polym 150:13–20. https://doi.org/10.1016/j.carbpol.2016.05.002
63. Bouklah M, Hammouti B, Lagrenée M, Bentiss F (2006) Thermodynamic properties of 2, 5-bis(4-methoxyphenyl)-1,3,4-oxadiazole as a corrosion inhibitor for mild steel in normal sulfuric acid medium. Corros Sci 48(9):2831–2842. https://doi.org/10.1016/j.corsci.2005.08.019
64. El-Lateef HMA, Abdallah ZA, Ahmed MSM (2019) Solvent-free synthesis and corrosion inhibition performance of ethyl 2-(1, 2, 3, 6-tetrahydro-6-oxo-2-thioxopyrimidin-4-yl)ethanoate on carbon steel in pickling acids: experimental, quantum chemical and Monte Carlo simulation studies. J Mol Liq 296:111800. https://doi.org/10.1016/j.molliq.2019.111800
65. Mourya P, Singh P, Tewari AK, Rastogi RB, Singh MM (2015) Relationship between structure and inhibition behaviour of quinolinium salts for mild steel corrosion: experimental and theoretical approach. Corros Sci 95:71–87. https://doi.org/10.1016/j.corsci.2015.02.034
66. Benhiba F et al (2020) Tetrahydropyrimido-triazepine derivatives as anti-corrosion additives for acid corrosion: chemical, electrochemical, surface and theoretical studies. Chem Phys Lett 743:137181. https://doi.org/10.1016/j.cplett.2020.137181
67. Goni LKMO, Jafar Mazumder MA, Quraishi MA, Mizanur Rahman M (2021) Bioinspired heterocyclic compounds as corrosion inhibitors: a comprehensive review. Chem Asian J 16(11):1324–1364. https://doi.org/10.1002/asia.202100201
68. Ahmed SK, Ali WB, Khadom AA (2019) Synthesis and investigations of heterocyclic compounds as corrosion inhibitors for mild steel in hydrochloric acid. Int J Ind Chem 10(2):159–173. https://doi.org/10.1007/s40090-019-0181-8
69. Imjjad A et al (2022) Corrosion inhibition of mild steel by aminobenzoic acid isomers in hydrochloric acid solution: efficiency and adsorption mechanisms. Appl Surf Sci 576:151780. https://doi.org/10.1016/j.apsusc.2021.151780
70. Zarrok H et al (2012) Gravimetric and quantum chemical studies of 1-[4-acetyl-2-(4-chlorophenyl)quinoxalin-1(4*H*)-yl]acetone as corrosion inhibitor for carbon steel in hydrochloric acid solution. J Chem Pharm Res 4(12):12
71. Lashkari M, Arshadi MR (2004) DFT studies of pyridine corrosion inhibitors in electrical double layer: solvent, substrate, and electric field effects. Chem Phys 299(1):131–137. https://doi.org/10.1016/j.chemphys.2003.12.019
72. Targema M, Obi-Egbedi NO, Adeoye MD (2013) Molecular structure and solvent effects on the dipole moments and polarizabilities of some aniline derivatives. Comput Theor Chem 1012:47–53. https://doi.org/10.1016/j.comptc.2013.02.020
73. Saha SK, Murmu M, Murmu NC, Obot IB, Banerjee P (2018) Molecular level insights for the corrosion inhibition effectiveness of three amine derivatives on the carbon steel surface in the adverse medium: a combined density functional theory and molecular dynamics simulation study. Surf Interfaces 10:65–73. https://doi.org/10.1016/j.surfin.2017.11.007
74. Lgaz H et al (2020) Assessing corrosion inhibition characteristics of hydrazone derivatives on mild steel in HCl: insights from electronic-scale DFT and atomic-scale molecular dynamics. J Mol Liq 308:112998. https://doi.org/10.1016/j.molliq.2020.112998
75. Murmu M, Saha SK, Bhaumick P, Murmu NC, Hirani H, Banerjee P (2020) Corrosion inhibition property of azomethine functionalized triazole derivatives in 1 mol L^{-1} HCl medium for mild steel: experimental and theoretical exploration. J Mol Liq 313:113508. https://doi.org/10.1016/j.molliq.2020.113508
76. Nwankwo HU, Olasunkanmi LO, Ebenso EE (2017) Experimental, quantum chemical and molecular dynamic simulations studies on the corrosion inhibition of mild steel by some carbazole derivatives. Sci Rep 7(1):2436. https://doi.org/10.1038/s41598-017-02446-0
77. Hadisaputra S, Purwoko AA, Savalas LRT, Prasetyo N, Yuanita E, Hamdiani S (2020) Quantum chemical and Monte Carlo simulation studies on inhibition performance of caffeine and its derivatives against corrosion of copper. Coatings 10(11):1086. https://doi.org/10.3390/coatings10111086

78. Sasikumar Y et al (2015) Experimental, quantum chemical and Monte Carlo simulation studies on the corrosion inhibition of some alkyl imidazolium ionic liquids containing tetrafluoroborate anion on mild steel in acidic medium. J Mol Liq 211:105–118. https://doi.org/10.1016/j.molliq.2015.06.052
79. Kr S, Hens A (2014) Molecular dynamics and density functional theory study on corrosion inhibitory action of three substituted pyrazine derivatives on steel surface. Can Chem Trans 3:1. https://doi.org/10.13179/canchemtrans.2014.02.04.0137